

Fermilab Library



0 1160 0052431 8

SSC-SDE-15

<p style="text-align: center;"><b>SSC-SDE</b> <b>SOLENOIDAL DETECTOR NOTES</b></p>
--

MUON DETECTOR MOMENTUM RESOLUTION  
November 15, 1989

Jim Wiss, Steve Errede

Jim Wiss  
Steve Errede  
University of Illinois  
November 15, 1989

## Muon Detector Momentum Resolution

This memo summarizes several calculations of momentum resolution for a possible magnetized iron muon detector for the SSC. Calculations were performed for the muon detector as a stand-alone system and for use in conjunction with a central detector and microstrip system. These calculations are all of the semi-analytic form (ie matrix methods) and ignore potentially important effects such as  $dE/dx$  loss, muon bremsstrahlung, pattern recognition etc. Ultimately we hope to test some of these conclusions using more detailed Monte Carlo simulation.

We begin with the discussion with the momentum resolution obtainable with a magnetized iron detector with detector planes uniformly spaced throughout the iron. We present some simple closed form approximate calculations which establish some general design principles for the use of a simplified segmented iron detector. The validity of the approximations is studied using some semi-analytic calculations.

Resolution calculations are made for the detector described in TABLE 1 and some simple variants of this detector. Finally we conclude by showing some results on the simulation of some interesting possible physics processes with an emphasis on the kinematic properties of detectable muons.

Here is summary of the detector layout considered:

TABLE 1

Detector	Radius	Number Planes	$\sigma(R\delta\phi)$	$\vec{B}$
SSD	.10 m - .14 m	5	$6\mu$	1.7 T
CTD	.60 m - 2.0 m	15	$150\mu$	1.7 T
Calorimeter	2.4 m - 4.8 m			
Flux Return	5 m - 6 m			- .62 T
Mu 1	4.92 - 4.98 m	4	$150\mu \rightarrow 1500\mu$	1.7 T
Mu 2	6.18 - 6.24 m	4	$150\mu \rightarrow 1500\mu$	1.7 T
Mu 3	8.90 - 8.96 m	4	$150\mu \rightarrow 1500\mu$	1.7 T
Mu 4	10.02 - 10.08 m	4	$150\mu \rightarrow 1500\mu$	1.7 T

### 1. Analytic Calculations of a Magnetized Iron Detector

It is possible to work out a simple closed form for the resolution of a magnetized iron muon detector subject to certain simplifying assumptions. We consider a detector which consists of a large number ( $N$ ) of uniformly separated planes with constant resolution ( $\sigma$ ) in a uniform magnetic field. ( $B$ ). The  $N$  planes span a total detector length  $L$  and are embedded in a medium with a  $X_0$  radiation length. We assume that the slope and intercept of incoming muons is very accurately measured by an upstream spectrometer with very little matter and very little multiple coulomb scattering (MCS). In this model, the muon system only measures momentum (curvature) of the muon trajectory in a one parameter fit. We assume that in this fit all planes are weighted equally. By way of contrast one can consider fits where the measured space points are fit using  $\chi^2$  constructed using the true coordinate covariance matrix which includes MCS contributions with their attendant correlations. We will refer to this latter fit as an MCS weighted fit.

Without the use of MCS weighting one can show in general that the momen-

tum resolution is of the form:

$$\frac{\sigma_P}{P} = \sigma_r \sqrt{\left(\frac{P}{P_*}\right)^2 + 1} \quad (1)$$

This simple form is not valid for the case of MCS weighted fits. For the particular detector described above, one can compute:

$$\sigma_r = \frac{.014}{.3 B \sqrt{L X_o}} \sqrt{\frac{130}{81}} \quad (2)$$

$$P_* = .014 \sqrt{\frac{L}{X_o}} \sqrt{N} \left(\frac{L}{\sigma}\right) \sqrt{\frac{13}{162}} \quad (3)$$

The units are GeV - meters - Tesla. These formula give the leading  $N$  approximations to the resolution but are fairly accurate once  $N$  exceeds 5.

One reaches several conclusions after examining Equations (1)  $\rightarrow$  (3). At low momenta ( $P \ll P_*$ ), where MCS dominates resolution effects, the fractional momentum error approaches a constant ( $\sigma_r$ ). At high momentum, the fractional momentum error grows proportional to momentum as is the case in any magnetic spectrometer. When MCS dominates, the fractional momentum error is essentially independent of detector properties such as the spacial resolution,  $\sigma$ , and number of planes and depends only on the gross properties of the iron slab such as the field, path length and radiation length ( $B$ ,  $L$ , and  $X_o$ ). Increasing the detector resolution (thus reducing  $\sigma$ ) or the increasing number of planes ( $N$ ) increases the effective momentum ( $P_*$ ) which is the momentum beyond which granularity effects rather than MCS effects dominate momentum resolution. Hence by upgrading the position detectors within the iron slab, one does not affect the momentum resolution at low momentum, but rather preserves the fractional error over a much larger range in muon momentum.

Here are some typical numbers from Eqn. (1)  $\rightarrow$  (3) to set the scale. For a 4 m thick, iron detector magnetized to 1.7 T, we expect a resolution of about

13.1 %. For the case of a (rather ambitious) 10 plane,  $\sigma = 150\mu m$  detector, the effective momentum would be  $P_* = 5000 \text{ GeV}$ .

Figure 1 is a computation of the resolution of a uniformly instrumented iron slab using matrix techniques. We assume a slab length of  $L = 4 \text{ m}$  and a field of 4 T. The curves give the fractional momentum error ( $\sigma/P$ ) as a function of the number of muon planes spaced uniformly within the 4 m slab. The curves are for 10 GeV muons (ie in the MCS limit -  $P \ll P_*$ ). The solid curves describe the resolution obtained for a one parameter fit (corresponding to the case where the slope and intercept are provided by external measurements); the dashed curves are for a full three parameter fit (all information is measured in the instrumented slab). The two upper curves describe unweighted fits; the two lower curves describe proper MCS weighting. Figure 1 shows that diminishing returns set in very quickly as a function of the number of planes embedded in the 4 m iron slab for the case of unweighted fits in accordance with Eqn. (1). Although all cases have comparable momentum resolutions in the range of 12 % or so, we note that the MCS weighted fit is able to make productive use of more planes and the slope and intercept constraint implied in the one parameter fit. By way of contrast, the no MCS weighted fit actually has better resolution when all information comes from the segmented iron detector -ie the constraints become information destroyers.

Figure 2 illustrates the effects of increased spacial resolution for the fractional momentum error ( $\sigma/P$ ) obtainable in a a 20 plane , 4 m , 1.7 T muon detector as a function of momentum. The solid curves are for unweighted 1 parameter fits; the dashed curves use MCS weighted fits. The curves are marked by the assumed space point error  $\sigma$ . At low momenta the fractional momentum error becomes independent of momentum and the space point error as anticipated in Equations (1)  $\rightarrow$  (3). The degradation at high momentum is significantly diminished by the use of a high resolution muon detector ( $\sigma = 150\mu m$ ). Figure 3 illustrates the effects of increasing the number of planes which instrument a 4 m slab for a muon detector of fixed detector resolution  $\sigma = 450\mu m$  by plotting the fractional

momentum error as a function of muon momentum for the case of a 10 plane and 80 plane system. Again the dashed curves represent MCS weighted fits while the solid curves are unweighted fits.

The semi-analytic (matrix) calculations more or less confirm the Eqn.(1) → (3). The use of MCS weighting clearly improves resolutions at roughly the 20 % level, and complicates the momentum dependence but isn't a really dramatic perturbation on the predictions of the analytic simplification. Eqn. (3) tells us that it is probably more economical to decrease  $\sigma$  rather than increasing  $N$  to forestall degradation in momentum at large  $N$ .

Up to this point we have considered muons which approach the muon detector at normal incidence ( $\theta = 90^\circ$  or  $\eta = 0$ ). If the muon is created at a polar angle  $\theta$  all relevant multiple scattering dimensions (lever arms as well as scattering thicknesses) will increase by a factor of  $1/\sin \theta$ . Since MCS spread through a slab is proportional to the length cubed, for a fixed muon total momentum, the MCS contribution to the coordinate covariance matrix will increase by a factor of  $1/\sin^3 \theta$ . In the limit of low P, then the resolution on the curvature ( $\mathcal{K} \equiv 1/P_\perp$ ) resolution will scale like:

$$\sigma_{\mathcal{K}} \propto \frac{1}{P \sin^{3/2} \theta} \propto \frac{1}{P_\perp \sqrt{\sin \theta}}$$

where one power of  $\sin \theta$  is absorbed in the  $P_\perp$  variable. In the language of Eqn. (1) → (3) we thus have the scaling law:

$$\frac{\sigma_{P_\perp}}{P_\perp} = \sigma_r(\theta) \sqrt{\left(\frac{P_\perp}{P_*(\theta)}\right)^2 + 1}, \quad \sigma_r(\theta) = \frac{\sigma_r(90^\circ)}{\sqrt{\sin \theta}} \quad (4)$$

and  $\sigma_r(90^\circ)$  is given by Equation (2).

At very large P, the MCS contribution to coordinate error becomes negligible compared to spacial resolution error and the fractional error in  $P_\perp$  must become

independent of  $\theta$  as is the case in the Central Tracking Detector. In light of Eqn. (4), we thus have the scaling law:

$$P_*(\theta) = \frac{P_*(90^\circ)}{\sqrt{\sin \theta}} \quad (5)$$

and  $P_*(90^\circ)$  is given by Equation (3).

Some of the ideas of Eqn. (4) and Eqn. (5) are illustrated by Figure 4 which gives the fractional  $P_\perp$  error as a function of  $P_\perp$  for a 4 meter thick, 1.7 T segmented iron detector, with 20 readout planes with  $\sigma = 450\mu m$  spacial resolution for the case of a  $\theta = 30^\circ$  (upper solid curve) and  $\theta = 90^\circ$  muon (lower solid curve). The dashed curves are for the cases where MCS weighting is employed. At low momenta, the  $\theta = 30^\circ$  case has  $\sqrt{2}$  worse resolution than the normal incident ( $\theta = 90^\circ$ ) case. The  $30^\circ$  and  $90^\circ$  cases approach each other as  $P$  increases.

## 2. The Muon System in Conjunction with a Central Tracker

Figure 5 shows the fractional momentum error ( $\sigma/P$ ) as a function of the muon momentum for the system described in TABLE 1 for with a full and partial complement of detectors. All fits assume a beam constraint and are MCS weighted. The dashed curves represent the momentum resolutions obtainable without using muon detector information. The upper dashed curve describes the momentum resolution without the use of SSD's ( silicon strip devices or microstrips); while the lower dashed curve describes the momentum resolution obtained using the central tracker in conjunction with the SSD's . The SSD system of TABLE 1 (which is an impressive detector with 5 planes of 6 micron RMS resolution) clearly does a lot in improving momentum resolution (a factor of 3 improvement at 1 TeV). At present, MCS in the SSD's is ignored.

The two solid curves of Figure 5 are drawn for a system using information from magnetized iron detector and a Central Tracking Detector. The upper solid

curve is for a system without an SSD; the lower solid curve is for a system with an SSD. Comparison of the upper dashed and upper solid curve of Figure 5, shows that the muon detector dramatically improves overall momentum resolution for systems with no SSD detectors (again by a factor of 3 at 1 TeV). For a detector with an SSD, the muon detector improves momentum resolution by a much more modest factor of about 1.7 at 1 TeV. Finally the dotted curve of Figure 5 shows the fractional momentum error for the muon as a stand alone system (although the beam constraint is still employed). Basically the muon system appears to serve as a break on the rapid deterioration of the momentum resolution of the Central Tracker Detector with increasing momentum. Presumably the asymptotic momentum resolution provided by the muon system described in TABLE 1 exceeds that of the Central Tracking Detector since the muon system has a much larger (ie 4 m) radial extent.

Finally Figure 6 investigates the effects of reducing the spacial resolution of the muon detector. This figure is drawn for a Central Tracking Detector with an excellent SSD system with no muon detector (dashed curve) with a muon detector with a spacial resolution of  $150 \mu m$  (lower solid curve) and a muon detector with a spacial resolution ten times worse -  $1500 \mu m$  (upper solid curve). The two dotted curves give the resolutions for the low and high resolution muon detectors operated in stand alone mode. A factor of 10 loss in muon detector spacial resolution seems to make the muon detector only half as effective in preserving momentum resolution for the combined system over a large momentum range.

### 3. Physics Process Simulations

We have begun a series of simulations of interesting physics processes which involve the production of final state muons. Eventually we hope to fully study the effectiveness of a muon system on such physics benchmarks. For the purposes of this memo, we thought it might be interesting to compute the  $P_{\perp}$  spectrum of such denizens of the standard model and some extensions. These simulations were made using ISAJET version 6.24 and include QCD  $P_{\perp}$  broadening effects.

Figure 7 shows the  $P_{\perp}$  spectra for conventional (91 GeV)  $Z^0 \rightarrow \mu^+\mu^-$ , heavy (500 GeV)  $Z_0 \rightarrow \mu^+\mu^-$  and a possible Higgs decay chain  $H \rightarrow Z^0Z^0 \rightarrow 4\mu$  where both 400 and 800 GeV Higgs are considered. In all cases we limited the muon pseudo-rapidity to be in the range of a barrel muon detector  $|\eta_{\mu}| < 1.5$ . The pseudo-rapidity distributions of the  $Z^0$ 's (both heavy and light tend to be flat over the range considered ( $|\eta_{\mu}| < 1.5$ ), while the Higg's  $\eta$  distribution tends to have a gentle peaking near  $\eta \approx 0$ .

For the processes considered above, the bulk of muon  $P_{\perp}$  spectrum lies below 500 GeV/c. In this region, Figure 5 shows us that the muon detector discussed makes some noticeable improvement in overall momentum resolution for a system without an SSD detector, but a rather marginal improvement over a system with a high quality SSD detector. The real improvements in overall  $P_{\perp}$  resolution provided by a magnetized muon detector occur at 1000 GeV  $P_{\perp}$  scales. On the other hand, the muon detector will still function as an excellent trigger component in this range.

We also note that with the large luminosities and cross sections available at the SSC, a rather large number of conventional Z's might be present at large  $P_{\perp}$ 's. The study of rare high high  $P_{\perp}$  muons such as those from high  $P_{\perp}$  Z decay will be greatly facilitated by the high resolution muon detector as described here and might serve as a major motivation for such a detector.

#### 4. Conclusions

We hopefully have demonstrated that a magnetized, segmented iron detector for muons can significantly improve overall muon momentum resolution when combined with a momentum information provided by a Central Tracker Detector at momenta of 1 TeV and beyond. These improvements are especially dramatic for the case of a system without SSD's (microstrip devices). In stand alone mode, a muon detector can provide a momentum resolution ( $\sigma/P$ ) in the range of 10 to 15 % up to about 2 TeV which should provide useful triggering information. As one increases the power of the muon detector by increasing spacial resolution or

increasing the number of readout layers, one does little to improve the resolution at low momenta but can dramatically extend the momentum range over which 10 to 15 % resolution is obtainable.

We are interested in continuing to investigate the performance of a muon detector similar to that described here with more detailed simulation tools, and with additional physics benchmarks which emphasize high  $P_{\perp}$  muons.

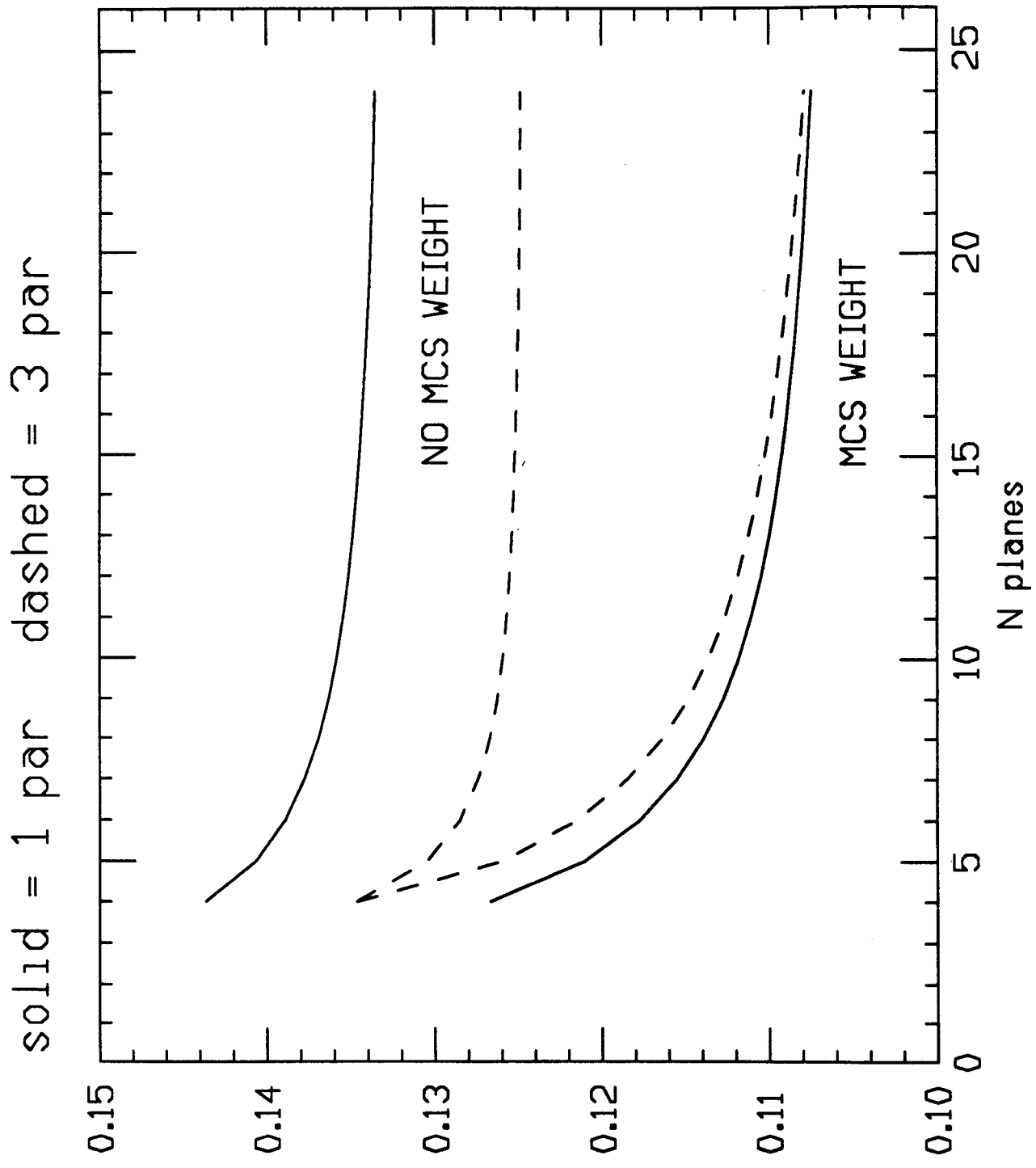


Figure 1

20 PLANES, 4 M, 1.7 KG

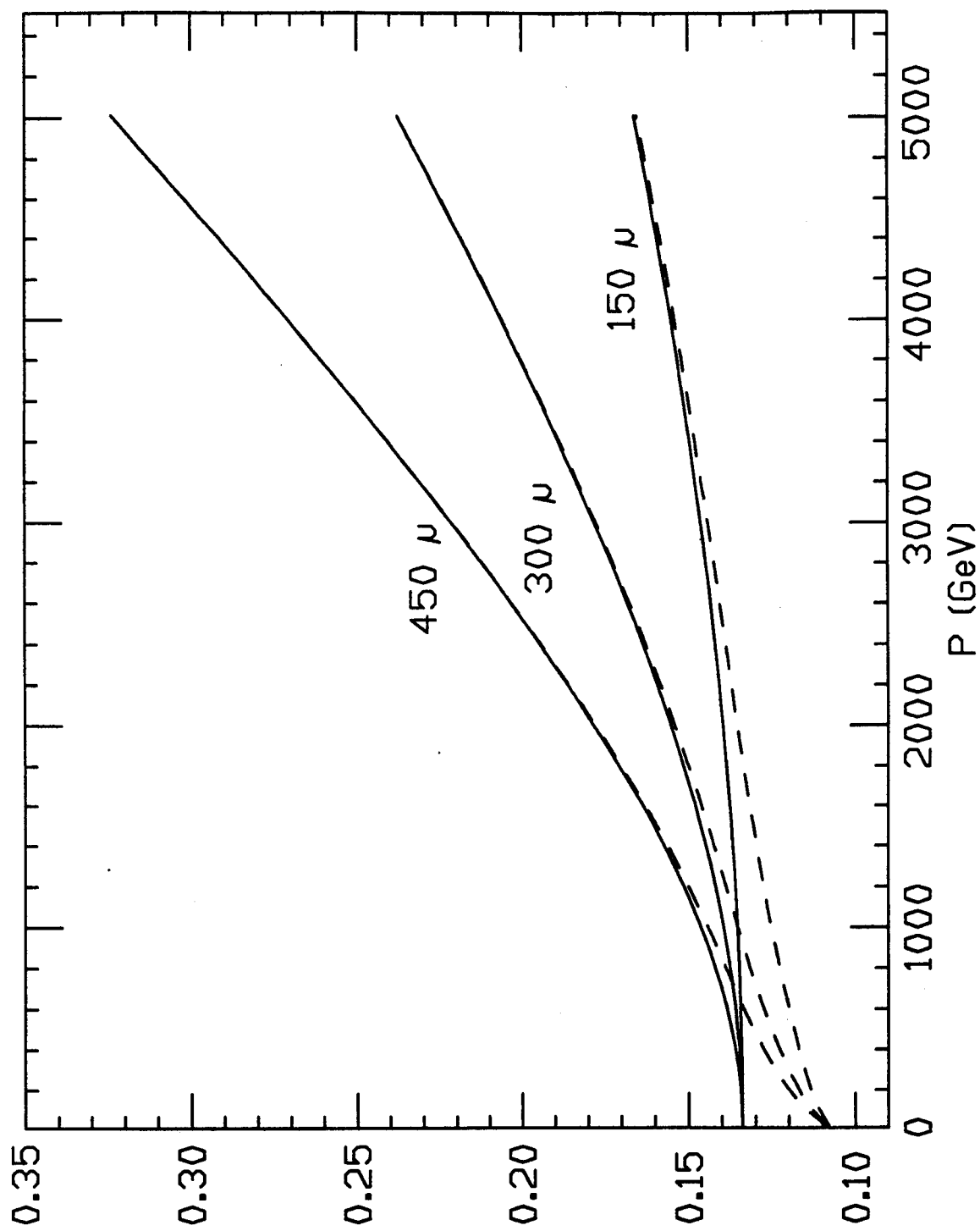


Figure 2

450  $\mu$ , 4 M, 1.7 kG

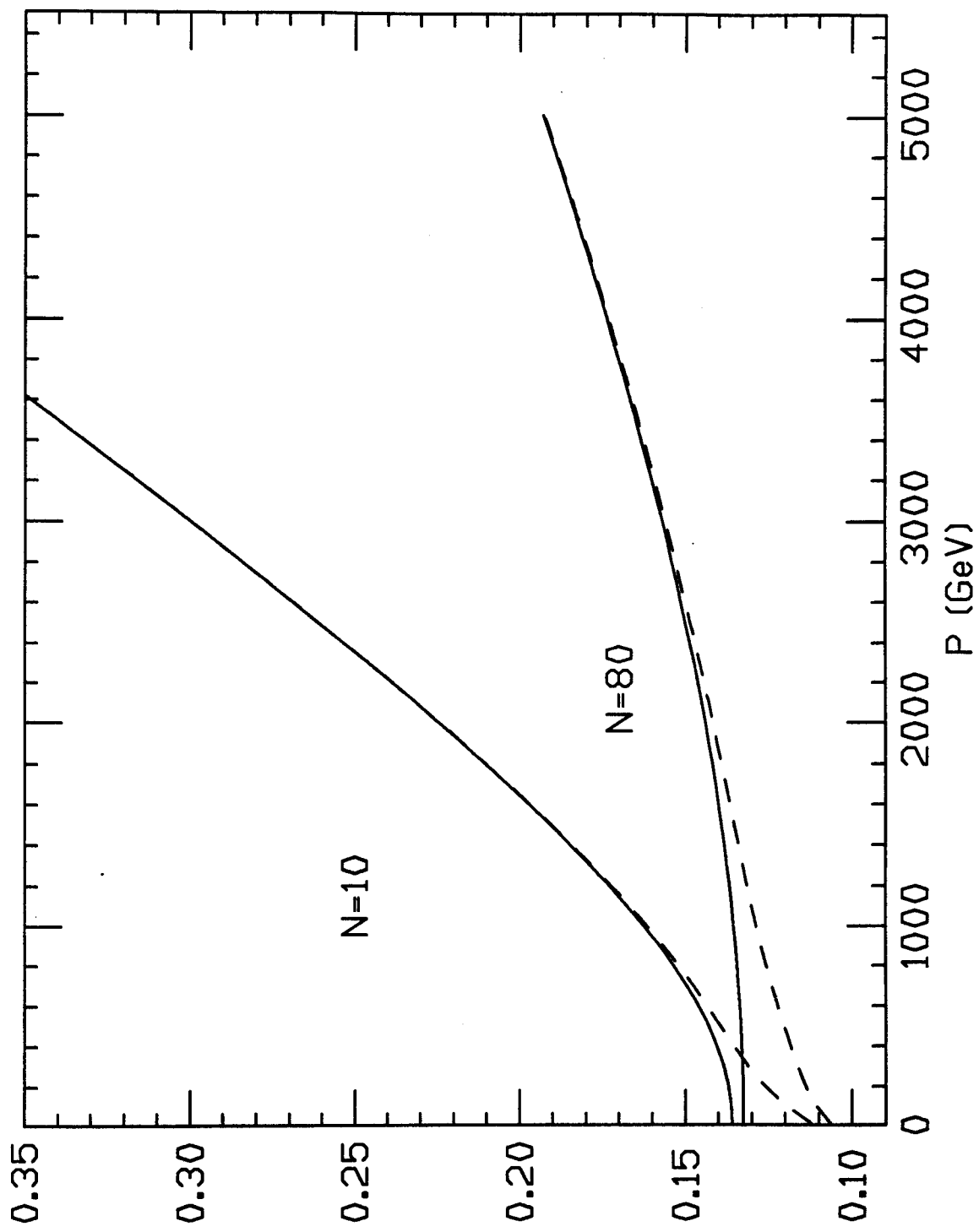


Figure 3

450  $\mu$  20 PLANES

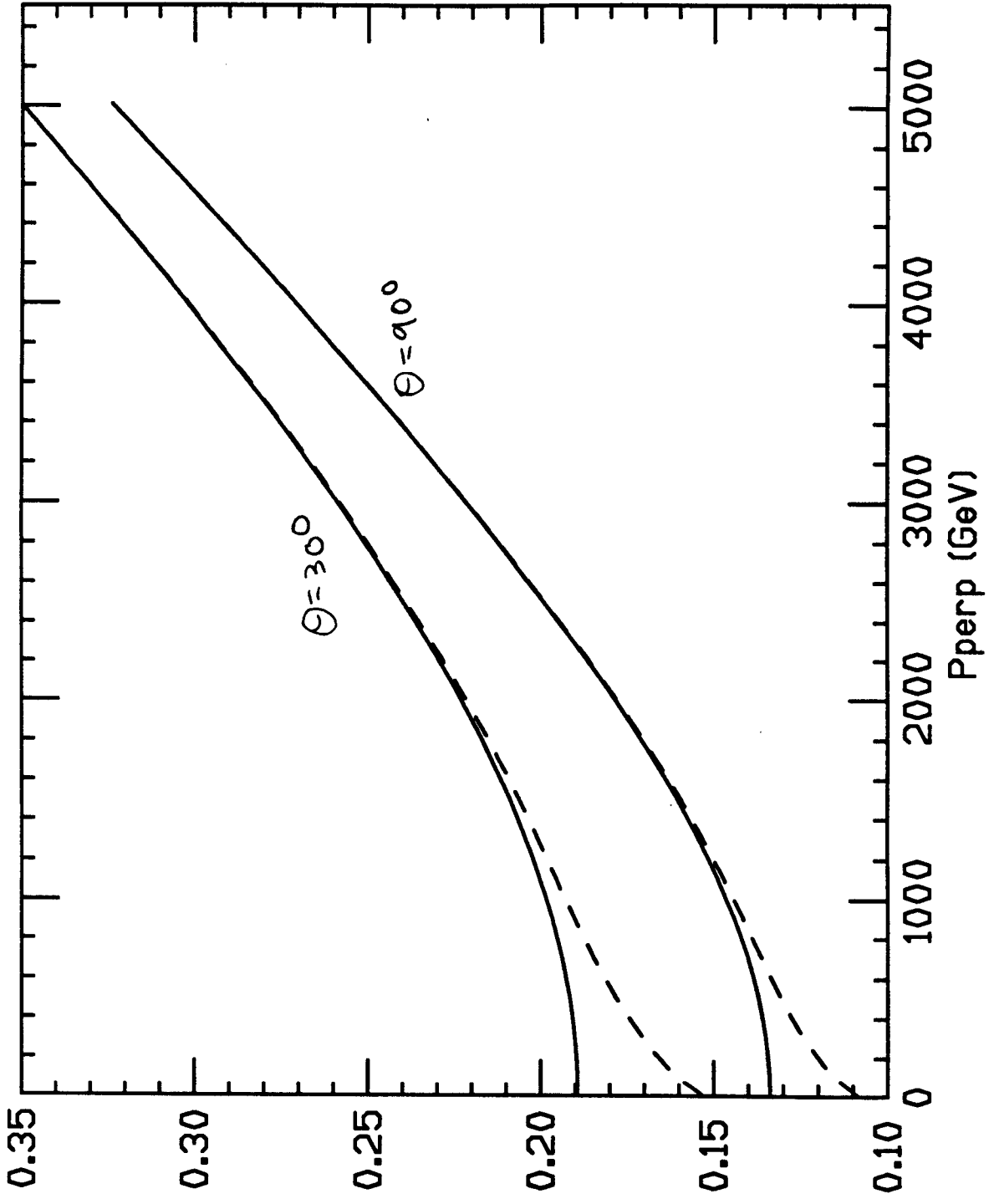


Figure 4

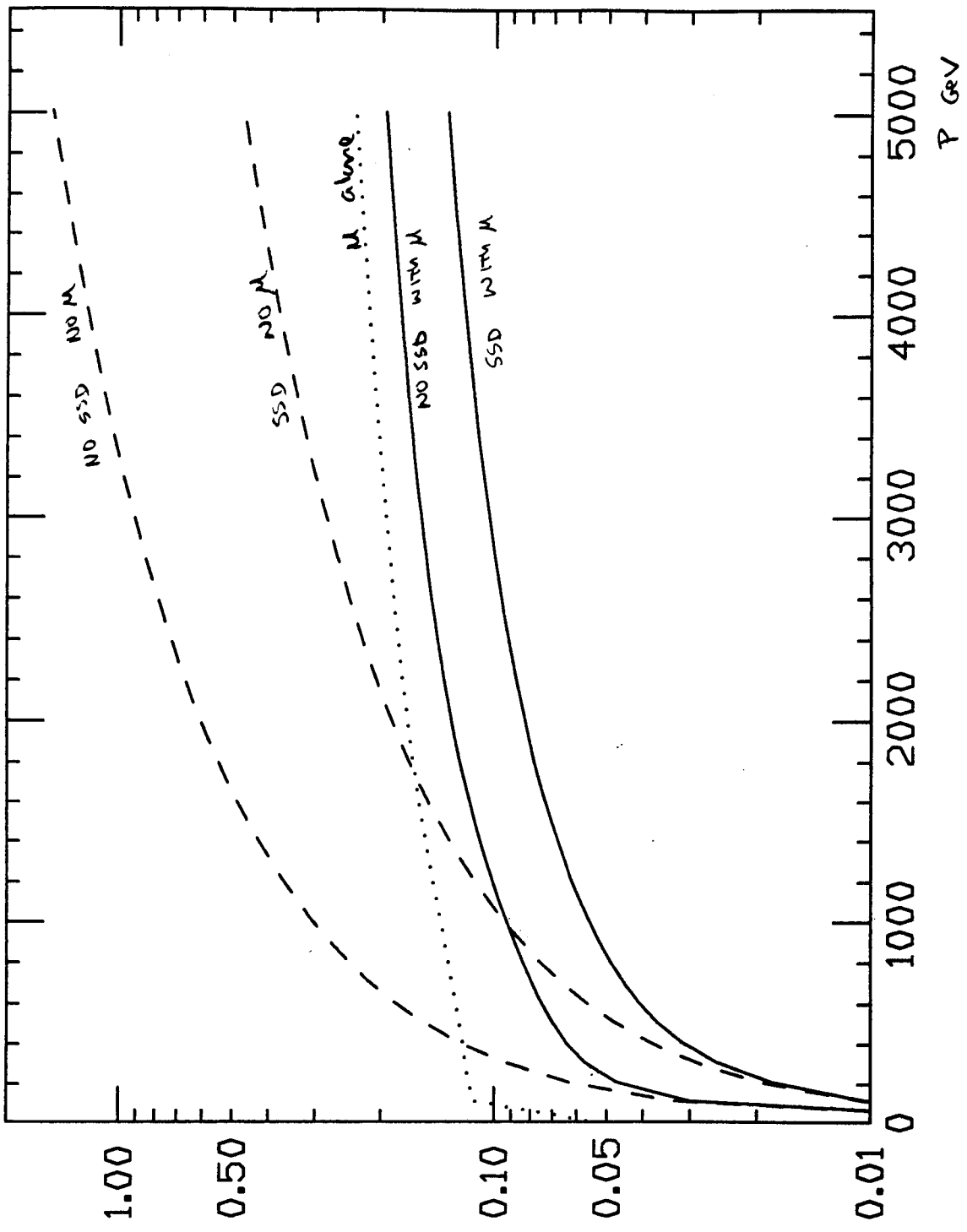


Figure 5

with SSD, 150  $\mu$  vrs 1500  $\mu$

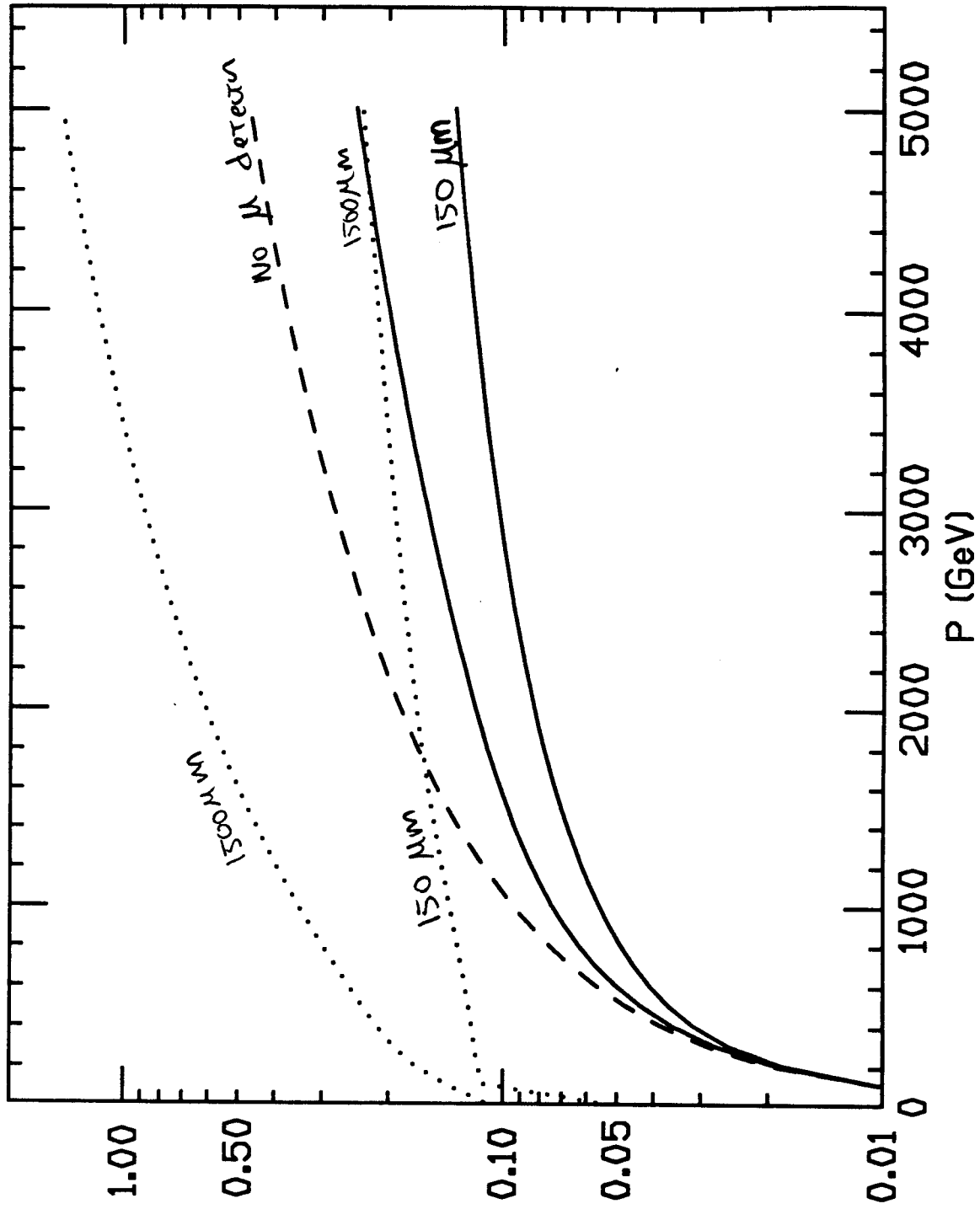
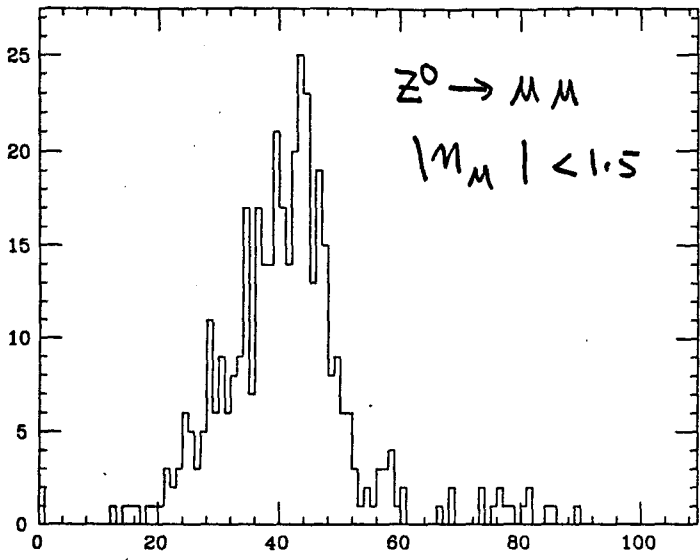
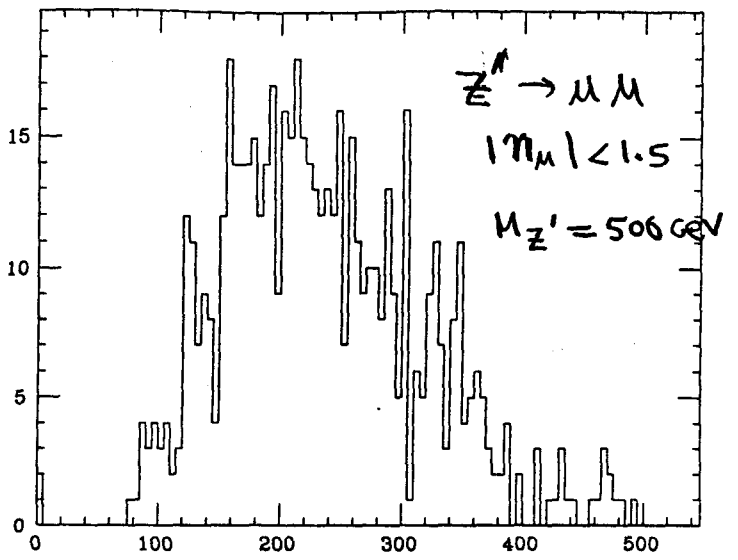


Figure 6

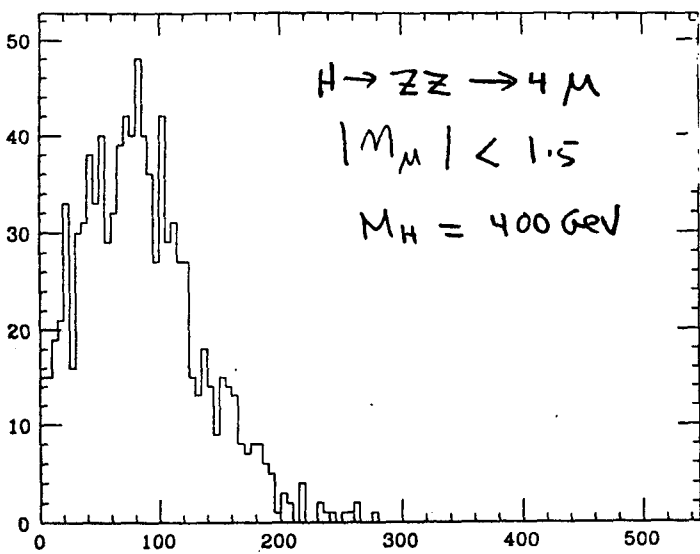
Muon Pt (GeV/c)



Muon Pt (GeV/c)



Muon Pt (GeV/c)



Muon Pt (GeV/c)

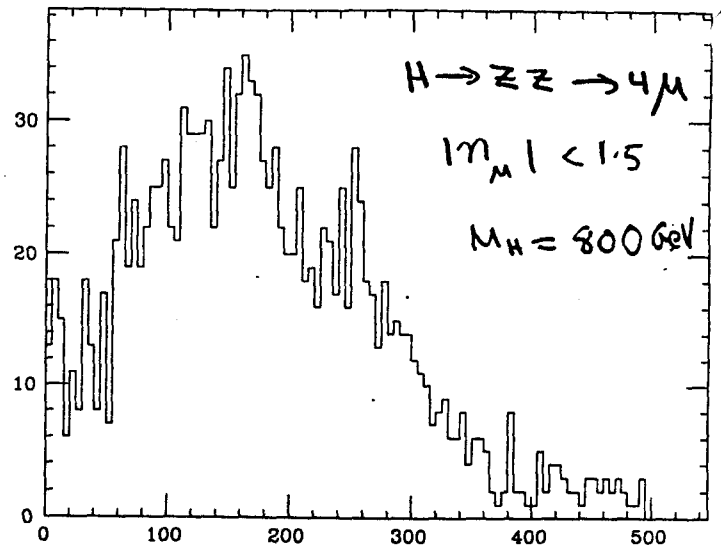


Figure 7